

OMEGA ICF experiments and preparation for direct drive ignition on NIF

R.L. McCrory^a, R.E. Bahr^a, R. Betti^a, T.R. Boehly^a, T.J.B. Collins^a, R.S. Craxton^a, J.A. Delettrez^a, W.R. Donaldson^a, R. Epstein^a, J. Frenje^b, V.Yu. Glebov^a, V.N. Goncharov^a, O.V. Gotchev^a, R.Q. Gram^a, D.R. Harding^a, D.G. Hicks^{b*}, P.A. Jaanimagi^a, R.L. Keck^a, J.H. Kelly^a, J.P. Knauer^a, C.K. Li^b, S.J. Loucks^a, L.D. Lund^a, F.J. Marshall^a, P.W. McKenty^a, D.D. Meyerhofer^a, S.F.B. Morse^a, R.D. Petrasso^b, P.B. Radha^a, S.P. Regan^a, S. Roberts^a, F. Séguin^b, W. Seka^a, S. Skupsky^a, V.A. Smalyuk^a, C. Sorce^a, J.M. Soures^a, C. Stoeckl^a, R.P.J. Town^a, M.D. Wittman^a, B. Yaakobi^a, J.D. Zuegel^a

^a Laboratory for Laser Energetics, University of Rochester,
Rochester, New York

^b Plasma Science and Fusion Center, Massachusetts Institute of Technology,
Cambridge, Massachusetts

United States of America

Abstract. Direct drive laser fusion ignition experiments rely on detailed understanding and control of irradiation uniformity, the Rayleigh–Taylor instability and target fabrication. The Laboratory for Laser Energetics (LLE) is investigating various theoretical aspects of a direct drive National Ignition Facility (NIF) ignition target based on an ‘all-DT’ design: a spherical target of ~ 3.4 mm diameter, with a 1–2 μm CH wall thickness and a DT ice layer of ~ 340 μm near the triple point of DT (~ 19 K). OMEGA experiments are designed to address the critical issues related to direct drive laser fusion and to provide the necessary data to validate the predictive capability of LLE computer codes. The cryogenic targets to be used on OMEGA are hydrodynamically equivalent to those planned for the NIF. The current experimental studies on OMEGA address the essential components of direct drive laser fusion: irradiation uniformity and laser imprinting, Rayleigh–Taylor growth and saturation, compressed core performance and shell–fuel mixing, laser–plasma interactions and their effect on target performance, and cryogenic target fabrication and handling.

1. Introduction

Direct drive ignition of inertial confinement fusion (ICF) targets [1] on the National Ignition Facility (NIF) is predicted to have higher gain (20–50) than indirect drive (~ 15) [2]. In this article the direct drive ICF experimental programme of the University of Rochester’s Laboratory for Laser Energetics (LLE) is summarized. LLE’s mission is to study the physics of direct drive ICF, through both experiments on the 60 beam, 30 kJ OMEGA laser system [3, 4] and simulations of the direct drive performance of NIF implosions [5, 6].

LLE’s theoretical programme is investigating various aspects of a direct drive NIF ignition target based on an ‘all-DT’ design: a spherical target of

~ 3.4 mm diameter, with a 1–2 μm CH wall thickness and a DT ice layer of ~ 340 μm near the triple point of DT (~ 19 K). The OMEGA experimental programme addresses the critical issues related to direct drive laser fusion and provides the necessary data to validate the predictive capability of LLE computer codes. The cryogenic targets to be used on OMEGA are hydrodynamically equivalent to those planned for the NIF. The current experimental studies on OMEGA address all of the essential components of direct drive laser fusion: irradiation uniformity and laser imprinting, Rayleigh–Taylor (RT) growth and saturation, compressed core performance and shell–fuel mixing, laser–plasma interactions and their effect on target performance, and cryogenic target fabrication and handling.

The primary constraint on direct drive ignition is the seeding and growth of the RT instability [1]. The RT instability occurs in both the acceleration

* *Current address:* Lawrence Livermore National Laboratory, Livermore, CA 94550, USA.

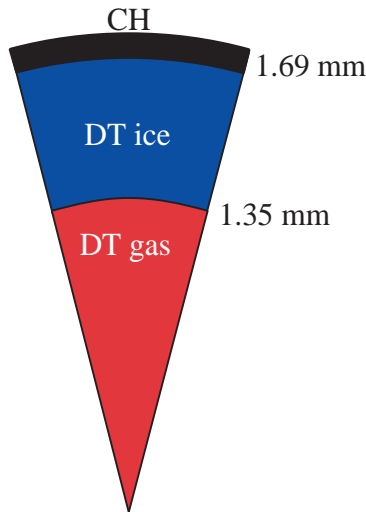


Figure 1. Schematic of the NIF all-DT direct drive target design.

and the deceleration phases of the target implosion. During the acceleration phase, the RT instability is seeded by the imprinting of laser non-uniformity, by target outer surface roughness, and by feed-out of inner surface perturbations after shock transit through the target. Additional shell distortions are caused by variations in power among the beams. The total amplitude of these perturbations must remain less than the in-flight shell thickness. Thus direct drive target designs must tolerate four sources of non-uniformity to ignite and burn: (1) inner DT ice roughness, (2) outside CH capsule finish, (3) drive asymmetry, and (4) laser imprinting.

2. NIF's direct drive target design

LLE's baseline NIF direct drive ignition design is based on a cryogenic DT target; it requires 1.5 MJ of laser energy and places the target on an $\alpha = 3$ isentrope (α is defined as the specific energy of the fuel divided by the Fermi degenerate specific energy) using a continuous pulse design. Recently significant progress was made in understanding the sensitivity of the NIF direct drive capsule designs to laser pulse shape characteristics [5, 6].

The baseline capsules are 3.4 mm in diameter and consist of a $340 \mu\text{m}$ layer of DT ice enclosed by a $1\text{--}2 \mu\text{m}$ thick plastic shell (Fig. 1). The continuous laser pulse used to drive these targets (shown in Fig. 2) consists of two distinct temporal regions: the foot and the main drive.

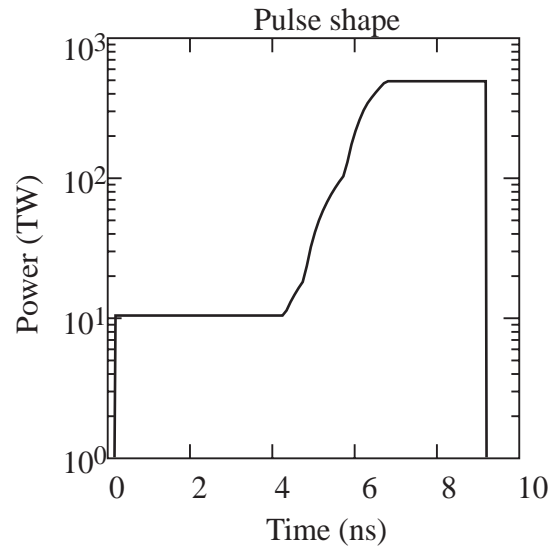


Figure 2. Pulse shape for the NIF direct drive ignition target.

The laser pulse creates two main shocks in the DT ice layer: the first is launched at the start of the pulse; the second is generated during the rise to the main drive intensity. The DT ice thickness and adiabat of the implosion determine the length and intensity of the foot. At a foot pulse intensity of ~ 10 TW, a 10 Mbar shock is launched through the DT ice. At the time of shock breakout at the rear surface of the DT ice, the pulse ramps up to the drive region, which lasts for 2.5 ns at a power of ~ 450 TW. This rapid rise in intensity generates pressures of approximately 80 Mbar and accelerates the DT ice inward. The highest gains are obtained when the second shock arrives at the DT ice inner surface just shortly after the first shock.

The baseline point design is predicted by 1-D calculations to attain a gain of 45, a neutron averaged ion temperature of 30 keV and a peak ρR of $\sim 1.3 \text{ g/cm}^2$. The peak in-flight aspect ratio (IFAR) of this design is 60, and the convergence ratio (initial target radius divided by the radius of the hot spot) is 28. The equation of state of the material, the ice thickness and the laser power determine the optimum timing of the two shocks.

Changing the length or intensity of the foot of the laser pulse controls the shock timing. A series of 1-D calculations were carried out to establish the sensitivity of the target performance to the duration and intensity of the foot. These simulations are summarized in Fig. 3. The gain drops when the power of the foot pulse or its duration is changed from optimum

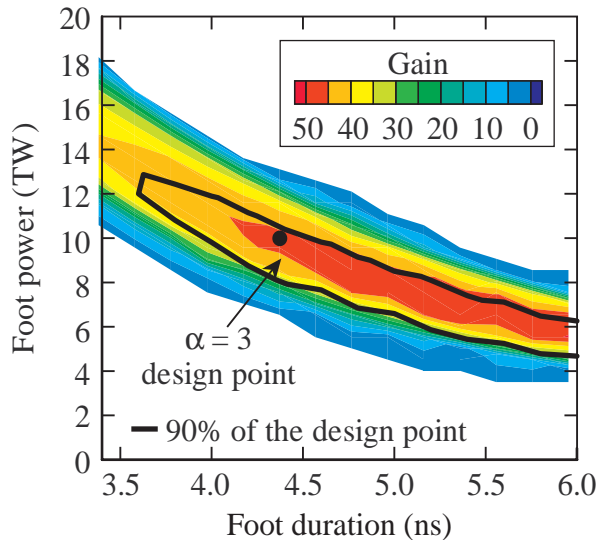


Figure 3. Contour plot of equal gain contours for the NIF direct drive capsule, with foot duration and foot power as the parameters. The black dot indicates the design point.

conditions. Such changes lead to a decompression of the inner part of the DT ice prior to the arrival of the second shock or to the coalescence of the two shocks prior to reaching the inner DT ice surface. Optimal timing between the two shocks can be maintained by trading the power of the foot with its duration. For a foot pulse duration of between 3.5 and 6 ns, the gain increases from about 40 to a maximum value of 50. The isentrope parameter α varies from 3.5 to 2.5 over that range. The design point at $\alpha = 3$ corresponds to a foot pulse duration of 4.4 ns and a foot power of 9.5 TW, resulting in a gain of ~ 45 (black dot in Fig. 3). The black contour line in Fig. 3 indicates the 90% gain contour around the design point and demonstrates acceptable tolerances on the foot power ($\pm 10\%$) and in the foot pulse duration (± 350 ps). For longer foot pulses, the gain is higher, but the isentrope is reduced, increasing the effect of the RT instability.

3. OMEGA cryogenic target designs

The basis for the OMEGA designs is the NIF direct drive $\alpha = 3$ design. One dimensional scaling arguments [7] are used to guide the design of the OMEGA cryogenic targets. The laser energy (E) required to contribute to a given plasma thermal energy scales roughly as the radius of the capsule (R) according to $E \sim R^3$. Since OMEGA delivers

30 kJ of energy, the radius of the OMEGA capsule will be approximately 30% of the NIF design. The corresponding OMEGA laser pulse is determined by noting that the time (t) or duration of the laser pulse scales as the confinement time and is roughly proportional to the radius of the target: $t \sim R$. The scaling of the peak power (P) in the laser pulse can be obtained from the energy and time scaling: $P \sim R^2$. Consequently the length of the laser pulse decreases from 9.25 ns in the NIF design to 2.5 ns for the OMEGA design. The peak power then scales to 32 TW. Processes other than hydrodynamics, such as radiation, thermal transport and thermonuclear burn, do not scale in a simple manner between the ignition designs and the OMEGA cryogenic designs. These energy scaled targets possess 1-D behaviour and instability growth similar to those of the ignition designs, thus meeting the requirement of hydrodynamic equivalence.

A series of detailed 1-D simulations were carried out to show that energy scaled OMEGA cryogenic capsules behave in a similar way to the NIF high gain optimized capsules. The two shock NIF design is compared with a scaled OMEGA capsule in Fig. 4. The difference in arrival time for the second shock in the OMEGA design compared with the NIF design is a consequence of lower laser energy absorption in the OMEGA design. Since the NIF designs typically have scale lengths that are 2 to 3 times longer than OMEGA, the absorption fraction for the NIF ignition designs is 60% while that of OMEGA is only 40%. Table 1 lists some of the key parameters calculated by 1-D simulations for the two designs. Note that the OMEGA and NIF designs have similar peak shell velocities, hot spot convergence ratios and IFARs.

Through the use of an instability postprocessor to the 1-D hydrocode LILAC [8–10] both the OMEGA and NIF direct drive designs are predicted to survive the acceleration phase. The NIF mix width is predicted to be approximately 35% of the overdense shell thickness, whereas the OMEGA mix width will be as much as 85% of the shell thickness. The OMEGA design has a lower safety factor for survival through the acceleration phase than the NIF point design.

The instability postprocessor cannot self-consistently determine the degradation of target yield for a given initial level of non-uniformity. ORCHID 2-D hydrocode simulations [5, 6] were used to determine the effect of non-uniformities of inner ice distortions at the start of the deceleration

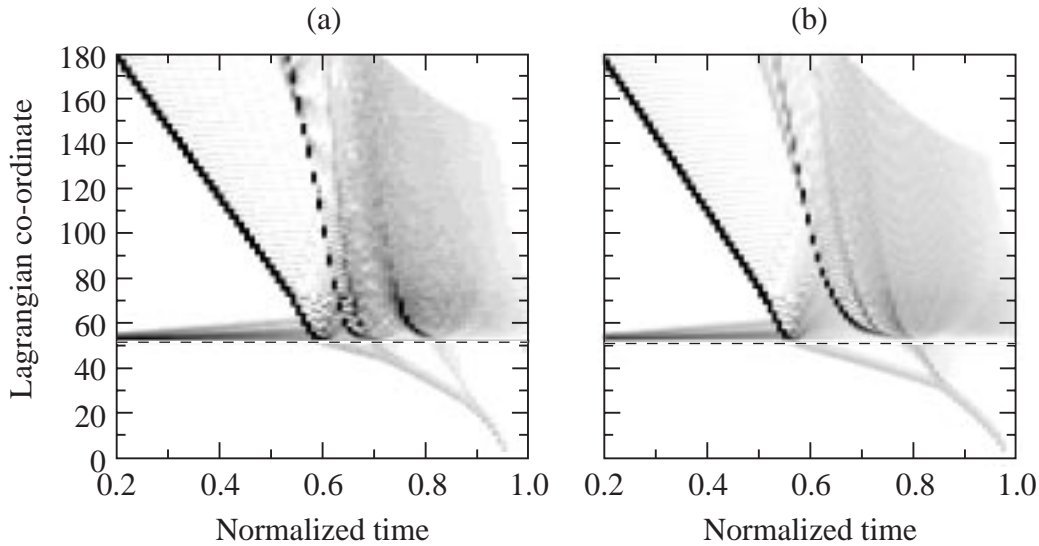


Figure 4. Shock propagation as shown by a contour map of the logarithmic derivative of the pressure as a function of normalized time and Lagrangian co-ordinate for (a) the NIF and (b) the OMEGA designs. Time has been normalized to the incident laser energy, with $t = 1.0$ corresponding to the end of the laser pulse. This allows the two designs to be compared at the same stage of the implosion. The darker shading indicates a larger pressure gradient and thus captures the position of the shocks. The OMEGA design shows similar timing for the first shock but a delayed second shock compared with the NIF design.

Table 1. Comparison of predicted 1-D parameters for NIF and OMEGA cryogenic target designs

	NIF	OMEGA
Absorption fraction (%)	60	40
Hydrodynamic efficiency (%)	11	12
Coupling efficiency (%)	7	4.5
Peak shell velocity (cm/s)	4.0×10^7	3.7×10^7
Hot spot convergence ratio	28	20
Peak in-flight aspect ratio	60	50
Peak areal density (mg/cm^2)	1200	300
Neutron averaged ion temperature (keV)	30	4
Neutron yield	2.5×10^{19}	1.8×10^{14}

phase on the overall target performance. These calculations indicate (Fig. 5) that OMEGA cryogenic targets with 1 THz_{UV}, 2-D smoothing by spectral dispersion (SSD) and 1 μm of inner ice surface roughness should obtain approximately 30% of the 1-D yield. Using the same analysis and similar target and laser uniformity levels, we predict that the $\alpha = 3$ direct drive ignition design will give a gain of 28 on the NIF, a reduction to 60% of the 1-D yield.

4. Irradiation uniformity

Various techniques, including 2-D SSD [11–14], distributed phase plates (DPPs) [15, 16], polarization smoothing (PS) utilizing distributed polarization rotators (DPRs) [17, 18], beam to beam precision power balance and beam overlap, are being used to achieve the high irradiation uniformity required for direct drive laser fusion experiments on OMEGA. These techniques will be applicable to the NIF and should be sufficient to reach the RMS non-uniformity level of 1% or less when the laser intensity is averaged over a few hundred picoseconds.

Figure 6 shows the effects of improvements in the on-target uniformity that have been implemented on OMEGA during the last year. The original SSD configuration consisted of IR bandwidths of $1.25 \times 1.75 \text{ \AA}$ with electro-optic modulators of 3 and 3.3 GHz. The spectral divergence was less than 50 μrad . In the last year, one of the modulators was replaced with a 10 GHz modulator, and the IR bandwidth was increased to $\sim 12 \text{ \AA}$, resulting in a UV bandwidth of $\sim 1 \text{ THz}$. To accommodate the higher bandwidth in frequency tripling, a third frequency conversion crystal has been added to all the OMEGA

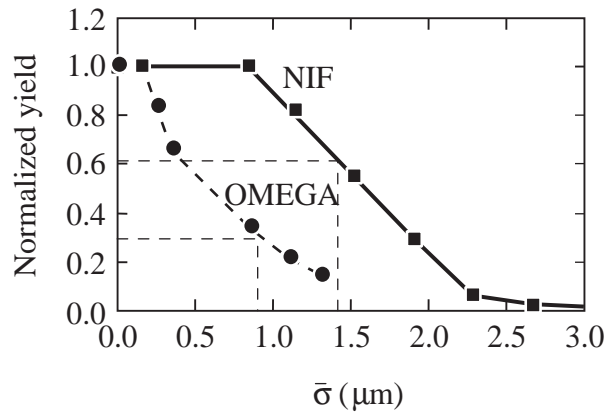


Figure 5. Predicted fusion yield (normalized to that of 1-D simulations) for NIF and OMEGA as a function of $\bar{\sigma}$, the effective non-uniformity at the start of the deceleration phase. The dashed lines correspond to the predicted $\bar{\sigma}$ levels for NIF and OMEGA (1.3 and 0.9 μm , respectively). OMEGA capsules suffer a larger reduction in yield for a given non-uniformity level than the NIF designs. This can be attributed to the OMEGA design's smaller hot spot radius compared with that of the NIF point design, which makes the OMEGA hot spot more easily disrupted by the penetration of cold spikes from the main fuel layer.

frequency conversion crystal assemblies [19, 20]. In addition, polarization wedges (DPRs) in the form of specially cut KDP crystals have been added to all the OMEGA beamlines.

The current configuration of SSD and PS (bottom curve in Fig. 6) results in overall smoothing of the irradiation uniformity to less than 1% RMS in less than 300 ps. The total non-uniformity in the long wavelength modes (spherical harmonic modes 11 to 30) can be smoothed to levels below 0.15%.

In addition to the application of individual beam smoothing such as SSD, it is also necessary to control the beam to beam power imbalance to levels below $\sim 5\%$ RMS. On OMEGA such control is implemented by the use of precision beam splitting and gain control on all beamlines. Precision calorimeters and high resolution optical streak cameras that can currently monitor 50 of the 60 OMEGA beams measure the power balance. Extension of this streak camera system to 60 beams is planned in the near future. Figure 7 shows a typical measurement of power balance for 40 of the beams carried out using the OMEGA multibeam streak camera system. Power imbalance

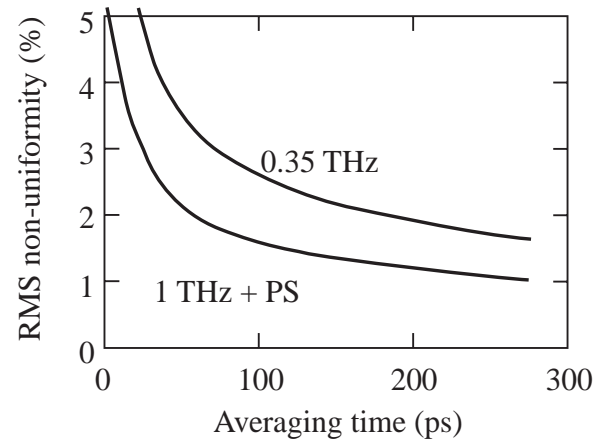


Figure 6. RMS non-uniformity as a function of time calculated assuming multiple beam overlap on a spherical target in the OMEGA 60 beam geometry. Curves are shown for two different configurations of SSD and PS. The current OMEGA configuration includes 1 THz 2-D SSD and PS.

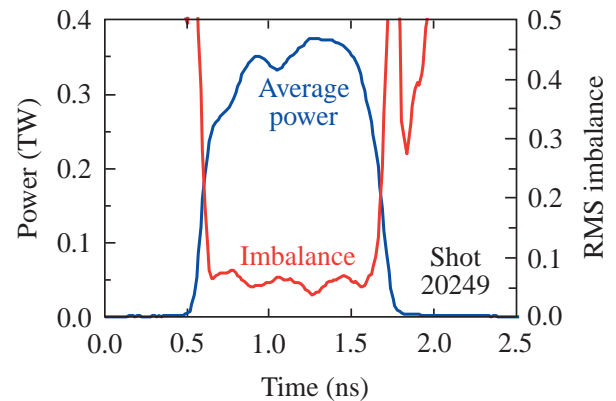


Figure 7. Average power and power imbalance as a function of time. These measurements are a 40 beam average with a 1 ns square pulse with 22 kJ on target.

of the order of $\sim 5\%$ RMS has been demonstrated for 1 ns square pulses.

All of these uniformity improvements are directly applicable to the NIF. As with OMEGA, the current pinhole specification for the NIF limits the angular spread of the beams to 50 μrad . The NIF optical design will need to be examined to determine if the pinholes can be opened further for direct drive experiments as was done on OMEGA. A comparison between NIF and OMEGA uniformity is shown in Fig. 8. The lower NIF non-uniformity level is due to the larger number of beams on NIF (192) than on OMEGA (60). It is expected that the NIF

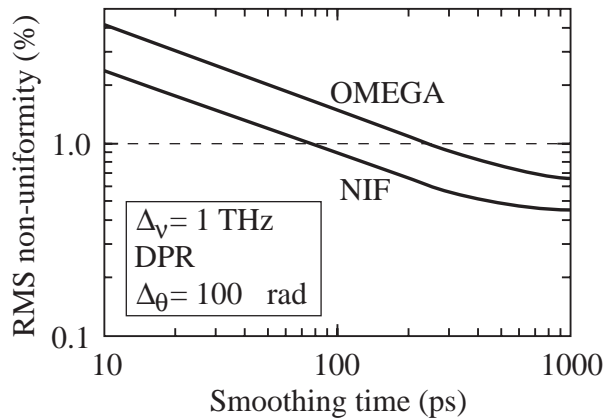


Figure 8. RMS non-uniformity plotted as a function of time for the NIF and for OMEGA, assuming 1 THz bandwidth and PS. All spherical harmonic modes between 5 and 500 are included in the calculation.

smoothing rate and uniformity level should be adequate for direct drive ignition experiments.

5. LLE's target physics research programme

LLE's target physics research programme combines all aspects of direct drive ICF. Specifically, the programme addresses: (a) early time phenomena such as plasma formation, laser-plasma instabilities, laser imprinting and shock formation; (b) RT growth, mitigation and saturation in the acceleration phase of the target compression; (c) RT growth during the deceleration phase; and (d) stagnation and core-shell mixing during peak compression. A variety of plasma diagnostic techniques are applied to study the physics of each of these phases of the target implosion.

The current OMEGA implosion experiments use CH shells that are energy scaled from NIF ignition target designs. Figure 9 schematically compares the typical OMEGA non-cryogenic targets with OMEGA cryogenic targets. In the non-cryogenic targets, the CH shell corresponds to the main fuel layer (DT ice) and the fill gas corresponds to the hot spot forming central DT gas.

The choice of shell thickness for the OMEGA non-cryogenic targets is primarily motivated by the fact that 1 mm dia., 20 μm thick CH shells driven by 1 ns square pulses have shell stability characteristics similar to the OMEGA $\alpha = 3$ cryogenic target designs (Fig. 10).

The goal of the OMEGA non-cryogenic target implosions is to study core conditions and mix characteristics. Several target diagnostics and target types are used in these experiments (as shown in Table 2).

Several experimental campaigns have been conducted using a single target configuration consisting of a 910–930 μm dia., 18–20 μm thick CH shell filled with 13–15 atm of D₂ or DT. These shells have been irradiated with ~ 23 kJ of UV energy in a 1 ns nearly square pulse. Several beam smoothing configurations have been used in these experiments, including 3 colour cycle, 0.35 THz SSD without PS and 1 colour cycle, 1 THz SSD with PS. The beam to beam power balance in the most recent set of experiments has averaged $<5\%$ RMS (Fig. 7).

Several nuclear measurements are made on these compression experiments to assess the fuel conditions at the time of thermonuclear burn. These include primary neutron yield; secondary neutron yield, secondary proton yield and spectra [22–24] (for D₂ filled targets); neutron averaged ion temperature; knock-on proton, deuteron and triton yield and spectra [25, 26] (for DT filled shells); and burn time history. In addition to neutron diagnostics, a large array of X ray imaging and spectroscopic diagnostics are also used in these experiments.

Typical charged particle measurements from experiments with full beam smoothing (1 THz, 2-D SSD with PS), including knock-on deuterons and knock-on protons (from DT filled capsule implosions) and secondary protons (from a D₂ filled capsule implosion), are shown in Fig. 11. The targets were ~ 920 μm dia., 19 μm thick CH shells filled with 15 atm of D₂ or DT and irradiated with 1 ns square pulses with 23 kJ of UV laser light. The top left part of Fig. 11 shows the knock-on deuteron spectrum from shot 20699; this spectrum indicates a fuel areal density of 16 mg/cm² (using a uniform ice block model [23]). At top right is the knock-on proton spectrum (from the CH shell) for shot 20699. This spectrum implies a shell areal density of 61 mg/cm². At the bottom of the figure is the integrated secondary proton spectrum from shots 20789, 20790 and 20791. These targets were D₂ filled shells similar in dimension and laser conditions to those of shot 20699. The secondary protons are produced with energies ranging from 12.5 to 17.5 MeV and are slowed down as they traverse the dense plasma. The total capsule areal density inferred from this measurement is 76 mg/cm², which is consistent with the total fuel and shell areal density measured on

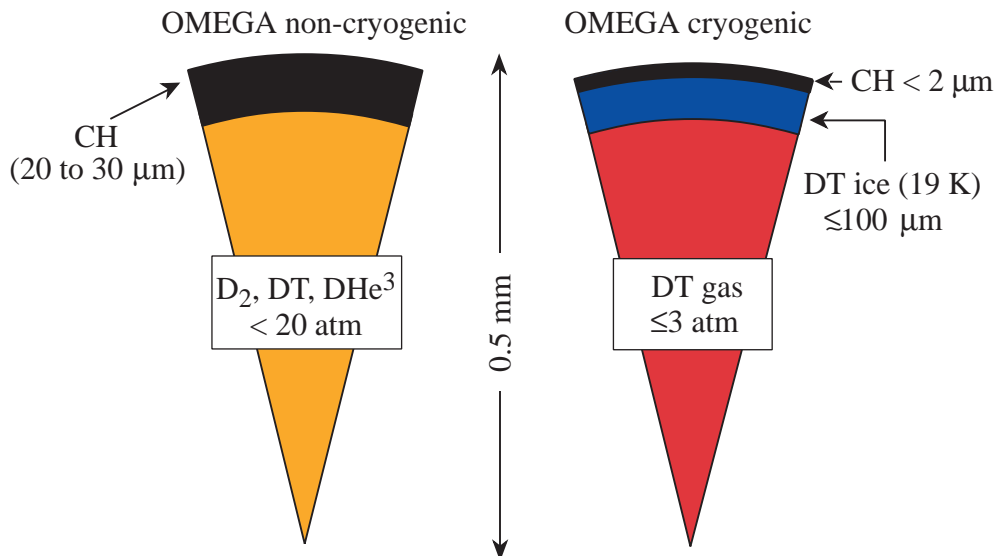


Figure 9. Sketch of typical OMEGA non-cryogenic and cryogenic implosion targets.

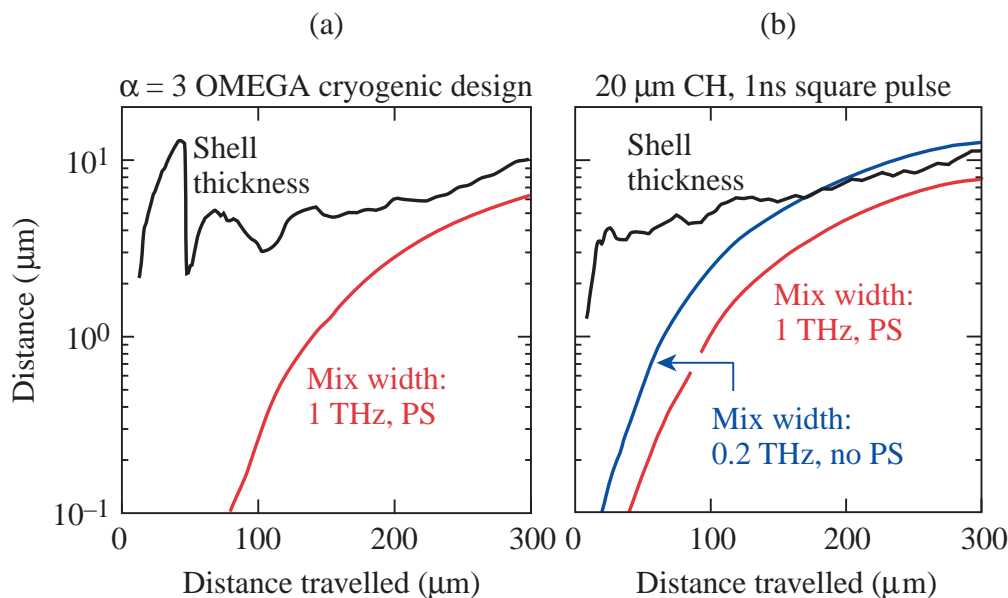


Figure 10. Comparison of the characteristic mix width and shell thickness for the OMEGA cryogenic design and the OMEGA warm capsule. The mix width is calculated using an instability model that includes Richtmyer–Meshkov, Rayleigh–Taylor and Bell–Plesset instabilities [8–10] and 3-D Haan saturation [21].

the DT shell of shot 20699. LILAC 1-D hydrocode simulations predict a fuel $\rho R \approx 17 \text{ mg/cm}^2$ and shell $\rho R \approx 64 \text{ mg/cm}^2$ for these implosions, in good agreement with the experimental measurements. The calculated fuel convergence ratio is ~ 15 . The

simulations also predict a primary yield approximately three times larger than measured.

Table 3 summarizes the comparative performance of these types of target (with D_2 or DT fills) for implosions with 1 THz 2-D SSD and PS and those

Table 2. OMEGA non-cryogenic target implosion types

Target type	Measured parameters
D ₂ and DT filled CH shells	Primary yield, fuel and shell ρR , T_i , bang time
CH shells with CD layers	Shell conditions and shell–fuel mix
CH shells with CHTi layers	Shell–fuel mix, shell integrity
D ₂ with Ar/Kr dopants	Average core fuel electron temperature/density

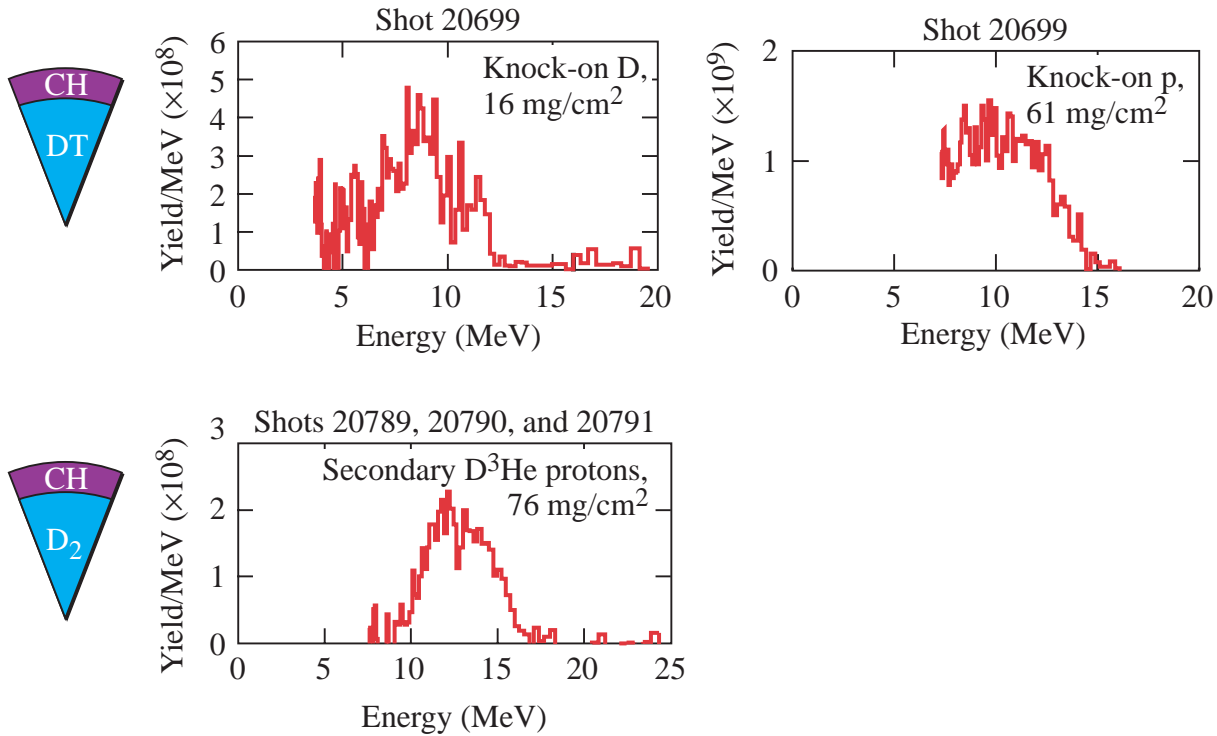


Figure 11. Sampling of particle spectra from a recent set of implosion experiments with improved beam smoothing using PS and 1 THz SSD.

with 3 colour cycle, 0.35 THz 2-D SSD without PS. Full beam smoothing significantly improves target performance.

6. Cryogenic targets on OMEGA

The first cryogenic capsule implosion using the OMEGA Cryogenic Target Handling System (CTHS) was carried out on 14 July 2000 (Fig. 12). The primary purpose of this shot was to test the fully integrated CTHS subsystems using a deuterium filled capsule. The capsule consisted of a 939 μm dia., 9 μm thick CD shell filled with deuterium to 1003 atm at

303 K, resulting in a 96 μm thick ice layer. To minimize the support structure mass and provide a relatively stiff support, the capsule was suspended by three 0.5 μm thick spider silk strands in a C shaped Be wire mount.

The energy on target was 16 kJ in a 1 ns square pulse. For this first test shot, fewer than half of the 60 OMEGA beams were used in order to protect the system from opposing beam damage in the event that the target was not in its prescribed location after shroud retraction. The ice layer thickness uniformity was not characterized. The primary DD neutron yield was $(3.5 \pm 0.3) \times 10^8$, and the ion temperature was 5.1 ± 1.3 keV.

Table 3. Summary of nuclear measurements on 19 μm thick CH shells filled with 15 atm of D_2 or DT and irradiated with 1 ns square pulses with 23 kJ of UV laser light

Measurement	3 cycle, 0.35 THz SSD	1 cycle, 1 THz SSD with PS
D_2 primary yield (10^{10})	9 ± 1	16 ± 1
T_i (D_2) (keV)	3.2	3.7
Secondary neutron ratio (10^{-3})	1.5 ± 0.4	2.5 ± 0.2
Secondary proton ratio (10^{-3})	1.4 ± 0.2	1.9 ± 0.2
DT primary yield (10^{12})	6 ± 1	11 ± 3
T_i (DT) (keV)	3.7	4.4
Knock-on ratio (10^{-5})	9 ± 3	13 ± 3

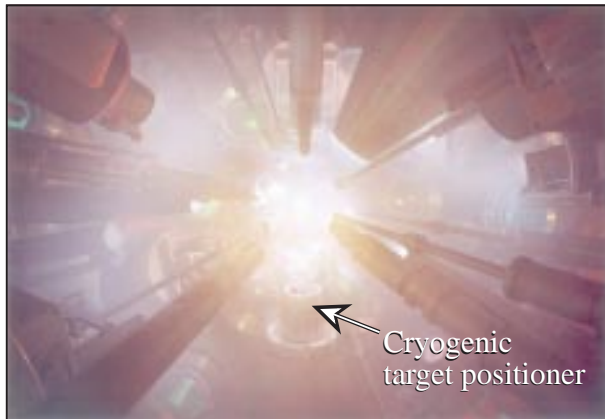


Figure 12. Photograph of the OMEGA target chamber during the first target shot using the CTHS. At the bottom centre of the photograph is the cryogenic target positioner.

This first test shot was the culmination of an intensive activation programme which focused on several issues: characterizing and minimizing target vibration; testing and refining the target manipulation at cryogenic temperatures; and testing the control software for the retraction of the thermal shroud (around the target) and the timing sequence for firing the laser. Issues that require further study are (1) the target vibration induced by the retracting shroud, and (2) the production and characterization of a smooth ice layer in a target.

A major source of target vibration is the initial shroud separation. The target has a resonant frequency of 284 Hz at 77 K and vibrates with a maximum amplitude of $\sim 20 \mu\text{m}$. During shroud retraction, however, the vibration can exceed $\sim 100 \mu\text{m}$. The velocity profile of the shroud retraction was programmed to minimize this vibration (Fig. 13).

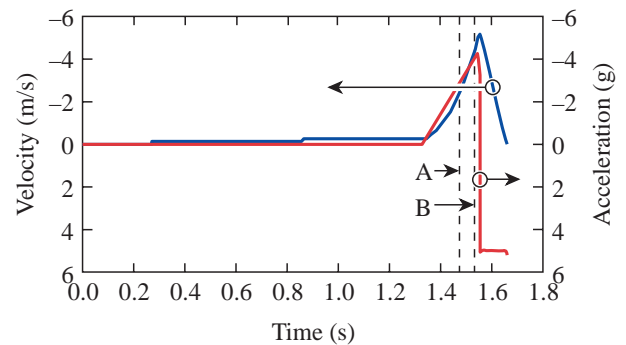


Figure 13. Acceleration time history of the shroud retraction is designed to minimize target vibration. The linear motor (LIM) translating the shroud initially accelerates at constant acceleration (-0.023g) until all the mating surfaces part. The LIM then accelerates to a maximum velocity of 5 m/s followed by a deceleration at 5g until the system comes to rest. The target is exposed at time A, and the laser fires 54 ms later at point B.

7. Summary

LLE is investigating various theoretical aspects of a direct drive NIF ignition target based on an all-DT design: a spherical target of $\sim 3.4 \text{ mm}$ diameter, with a $1\text{--}2 \mu\text{m}$ CH wall thickness and a DT ice layer of $\sim 350 \mu\text{m}$ near the triple point of DT ($\sim 19 \text{ K}$). OMEGA experiments are designed to address the critical issues related to direct drive laser fusion and to provide the necessary data to validate the predictive capability of LLE computer codes. Future cryogenic targets used on OMEGA will be hydrodynamically equivalent to those planned for the NIF. The current experimental studies on OMEGA address the essential components of direct drive laser fusion: irradiation uniformity and laser imprinting,

RT growth and saturation, compressed core performance and shell–fuel mixing, laser–plasma interactions and their effect on target performance, and cryogenic target fabrication and handling. Recent improvements in irradiation uniformity resulted in significant improvements in target performance, with fuel and shell ρR in these experiments nearly equal to 1-D hydrocode predictions.

8. Acknowledgements

This work was supported by the US Department of Energy (DOE) Office of Inertial Confinement Fusion under Cooperative Agreement DE-FC03-92SF19460, the University of Rochester, and the New York State Energy Research and Development Authority. The support of the DOE does not constitute an endorsement by the DOE of the views expressed in this article.

References

- [1] Bodner, S.E., et al., *Phys. Plasmas* **5** (1998) 1901.
- [2] Lindl, J.D., *Phys. Plasmas* **2** (1995) 3933.
- [3] Boehly, T.R., et al., *Opt. Commun.* **133** (1997) 495.
- [4] Soures, J.M., et al., *Phys. Plasmas* **3** (1996) 2108.
- [5] “OMEGA cryogenic target designs”, LLE Review **82**, pp. 49–55, NTIS document No. DOE/SF/19460-344 (2000). Copies may be obtained from the National Technical Information Service, Springfield, VA 22161, USA.
- [6] “Direct-drive target designs for the National Ignition Facility”, LLE Review **79**, pp. 121–130, NTIS document No. DOE/SF/19460-317 (1999). Copies may be obtained from the National Technical Information Service, Springfield, VA 22161, USA.
- [7] Brueckner, K.A., Jorna, S., *Rev. Mod. Phys.* **46** (1974) 325.
- [8] Goncharov, V.N., *Self-Consistent Stability Analysis of Ablation Fronts in Inertial Confinement Fusion*, PhD Thesis, Univ. of Rochester, NY (1998).
- [9] Goncharov, V.N., et al., Modeling hydrodynamic instabilities in inertial confinement fusion targets, *Phys. Plasmas* (in press).
- [10] “Stability analysis of directly driven NIF capsules”, LLE Review **81**, pp. 1–5, NTIS document No. DOE/SF/19460-335 (1999). Copies may be obtained from the National Technical Information Service, Springfield, VA 22161, USA.
- [11] Skupsky, S., et al., *J. Appl. Phys.* **66** (1989) 3456.
- [12] Skupsky, S., Craxton, R.S., *Phys. Plasmas* **6** (1999) 2157.
- [13] “Two-dimensional SSD on OMEGA”, LLE Review **69**, pp. 1–10, NTIS document No. DOE/SF/19460-152 (1996). Copies may be obtained from the National Technical Information Service, Springfield, VA 22161, USA.
- [14] Rothenberg, J.E., *J. Opt. Soc. Am. B* **14** (1997) 1664.
- [15] Kessler, T.J., et al., “Phase conversion of lasers with low-loss distributed phase plates”, *Laser Coherence Control: Technology and Applications* (Powell, H.T., Kessler, T.J., Eds), Vol. 1870, SPIE, Bellingham, WA (1993) 95–104.
- [16] Lin, Y., Kessler, T.J., Lawrence, G.N., *Opt. Lett.* **21** (1996) 1703.
- [17] Tsubakimoto, K., et al., *Opt. Commun.* **91** (1992) 9.
- [18] Gunderman, T.E., et al., “Liquid crystal distributed polarization rotator for improved uniformity of focused laser light”, *Conf. on Lasers and Electro-Optics*, Vol. 7, Technical Digest Series, Optical Society of America, Washington, DC (1990) 354.
- [19] Eimerl, D., et al., *Opt. Lett.* **22** (1997) 1208.
- [20] Babushkin, A., et al., *Opt. Lett.* **23** (1998) 927.
- [21] Haan, S.W., *Phys. Rev. A* **39** (1989) 5812.
- [22] Glebov, V.Yu., et al., Secondary-neutron-yield measurements by current-mode detectors, *Rev. Sci. Instrum.* (in press).
- [23] Li, C.K., et al., *Phys. Plasmas* **7** (2000) 2578.
- [24] Seguin, F., et al., Using secondary proton spectra to study imploded D₂-filled capsules at the OMEGA laser facility (in preparation).
- [25] Radha, P.B., et al., *Phys. Plasmas* **7** (2000) 1531.
- [26] Li, C.K., et al., Study of direct-drive, DT gas-filled plastic capsule implosions using nuclear diagnostics at OMEGA (in preparation).

(Manuscript received 4 October 2000)

Final manuscript accepted 25 January 2001)

E-mail address of J.M. Soures: jsou@lle.rochester.edu

Subject classification: L0, Ie